

RESEARCH PAPER

## Au /Cu Nanoparticles with Study the Structural Properties via Effect against Bacteria

Eman M. Sulaiman <sup>1</sup>, Rejwan K. Ibrahim <sup>2</sup>, Amna K. Faraj <sup>3</sup>, Noor M.Saadoon <sup>1\*</sup>, Fadhil A. Kareem <sup>4</sup>, Ahmed J. Jasim <sup>5</sup>

<sup>1</sup> University of Technology, Iraq

<sup>2</sup> Centre of Nanotechnology and Advanced Material, University of Technology, Iraq

<sup>3</sup> Department of Quality Assurance and University Performance, University of Technology, Baghdad, Iraq

<sup>4</sup> Central Committee for Scientific Promotions, University of Technology, Iraq

<sup>5</sup> Department of Medical Engineering, University of Technology, Iraq

### ARTICLE INFO

#### Article History:

Received 15 September 2024

Accepted 19 December 2024

Published 01 January 2025

#### Keywords:

Bacteria efficiency

Copper

Gold nanoparticles

Laser ablation

### ABSTRACT

This study uses economical and ecologically friendly techniques to create gold nanoparticles (Au-NPs) and copper nanoparticles (Cu-NPs) utilizing distilled water (DW) solution and the liquid pulse laser ablation (PLAL) technique with a wavelength of 1064 nm and varying laser intensities. Using X-ray diffraction (XRD) and absorption spectrometry, the characteristics of Au-NPs and Cu NPs as well as Au-CuNPs were investigated. The results indicated that a crystal structure for gold (Fcc) had formed. The appearance of the surface plasmon resonance (SPR) peak at 523 nm in the UV visible spectrum in the Uv-Vis data demonstrated the creation of Au NPs. Cu NPs and Au NPs nanoparticles (Au-CuNPs) have antibacterial properties against E. coli and Staph aureus. This is because the high surface-to-volume ratio offers provides a more effective means of enhancing bacterial activity as measured by the area of inhibition.

### How to cite this article

Sulaiman E., Ibrahim R., Faraj A., Saadoon N., Kareem F., Jasim A. Au /Cu Nanoparticles with Study the Structural Properties via Effect against Bacteria. J Nanostruct, 2025; 15(1):301-309. DOI: 10.22052/JNS.2025.01.029

### INTRODUCTION

There are numerous opportunities to investigate nanoparticles' theranostic role in molecular imaging thanks to recent developments in nanotechnology and nanomaterials. In molecular imaging, gold nanoparticles have been widely used as contrast agents and drug delivery systems. This is because of the exceptional qualities of gold nanoparticles, such as their high chemical stability, facile bioconjugation with different molecules, and outstanding biocompatibility with human cells. Gold nanoparticles can be created using different processes including conventional chemical

synthesis, radiation technologies, electrochemical, bio-synthesizing and pulsed laser ablation in liquid (PLAL) [1,2]. Although there are several approaches for creating gold nanoparticles, each has pros and cons of its own. PLAL is the most widely used process for creating nanomaterials because it is easy to use, inexpensive, efficient, and environmentally benign [3–5].

The solid gold target is submerged in a liquid solution during the synthesis of gold nanoparticles. Through the liquid medium, the laser beam ablates the target surface and deposits energy on it, causing the target material to melt and heat

\* Corresponding Author Email: [mae.visit.04@uotechnology.edu.iq](mailto:mae.visit.04@uotechnology.edu.iq)



locally. The target material's surface is where ejection and evaporation mechanisms take place, and the atoms, clusters, and droplets that are released cool down to form gold nanoparticles. [6-7].

When these two substances react, gold nanoparticles in liquid solution are created. There is no chemical agent reduction or use of toxicity surfactants in the PLAL approach. Consequently, the purity, quality, and homogeneity of gold nanoparticles are preserved by the PLAL process. [8-9].

A superior platform and flexibility for direct conjugation with biocompatible polymers are offered by the purity of gold nanoparticles and their bigger, distinct, contamination-free surface [4,7,10]. The bacteria will die as a result of the contents of AuNPs leaking through the outer membrane and peptidoglycan layer after binding to the bacterial membrane. [11]. When comparing with copper nanoparticles (CuNPs).

## MATERIALS AND METHODS

### *Method and materials*

Laser ablation was performed using a switched Nd-YAG laser system that produced pulses with a wavelength of 1064 nm, a pulse width of 10 ns, a repetition rate of 1 Hz, a maximum energy per pulse of 700 mJ, and an effective beam diameter of 2 mm. Even if the common features are still present, laser energy is focused on a solid object that has been submerged in liquid. It is anticipated that the liquid will be clear at the laser wavelength; if not, the absorption of laser radiation in the liquid will impair the focalization of the beam. Working with the liquid's free surface is the simplest approach since it removes extra reflection at the "covering glass/air" interface. However, a window that is transparent at the laser wavelength needs to be utilized to cover the liquid when working with volatile liquids like ethanol or acetone. The liquid or solution has a significant impact on the production of nanoparticles in the PLAL process. In addition to serving as a liquid medium for suspending the source particles, solution has a significant impact on the size, stability, and production yield of the NPs that are produced. Furthermore, potential chemical processes like oxidation or reduction [12] might take place. The size distribution and characteristics of the NPs could then be significantly impacted by the solution, additives included or not.

### *The PLAL Mechanism*

There are several physical mechanisms involved in the PLAL mechanism. The metal target absorbs the laser's photon energy during the PLAL process, which causes the irradiated area to heat up and become photoionized. The energy from the ablation laser is transformed into an excitation of the metal target's electron bonding, which breaks the bonding at the threshold energy level. These liberated electrons absorb incoming laser photons and further ionize the target material, according to the principle of Inverse Bremsstrahlung [13]. Additionally, the explosive process, vaporization, and boiling all happened at the same time. Some of the metal surfaces are removed as liquid droplets, solid fragments, plasma plumes, or vapors. The absorbed energy determines the amount of ablated area.

### *The PLAL Synthetizations Method*

According to a recent study, the PLAL process is the most persuasive and promising method for creating gold nanoparticles [14]. In certain investigations, gold nanoparticles were created using the PLAL approach using pulse laser Neodymium-doped Yttrium Aluminum Garnet (Nd: YAG) [15]. The Nd: YAG laser was chosen because of its widespread availability and high efficiency. In the PLAL approach, gold nanoparticles.

### *Laser Parameters*

The shape, structure, diameter, size, and distribution of produced gold nanoparticles are influenced by the laser's energy, wavelength, fluency, pulse repetition, and ablation time. The gold nanoparticles that PLAL generated had a spherical form [17].

Because of its enormous surface area, this shape is crucial for providing conjugation with other molecules, including peptides, biomarkers, and medicines in molecular imaging. Furthermore, the size distribution of gold nanoparticles refers to their quantity and pattern in a liquid media, such as uniform or clusters, whereas the diameter of gold nanoparticles refers to their size. [18].

### *Preparation of Au- cu nanoparticles*

The laser ablation process, which is regarded as one of the most crucial techniques for creating nanomaterials and as an environmentally friendly approach, was used to create gold nanoparticles [2-3]. A gold pellet was submerged in three

milliliters of deionized water to create gold nanoparticles using a Nd:YAG laser. Laser radiation with an energy of 700 mJ and a wavelength of 1065 nm at one hertz was then focused on the target's surface. Following the preparation of the suspended gold nanoparticle solution, a high-purity copper pellet was submerged in the Au NPs solution, and the copper material's surface was then exposed to laser radiation.

### RESULT AND DISSOCIATION

#### X-ray diffraction test (XRD) X-ray diffraction

X-ray diffraction (XRD) was used on samples generated with a Shimadzu 6000 X-ray diffraction equipment at a wavelength of  $\lambda = 1.54060 \text{ \AA}$  and an effort difference of 40 KV For Au-NPs made using the laser extraction approach at an energy of 700 mJ, Fig. 2 displays the X-ray diffraction patterns (XRD). The characteristic peaks of Au-NPs were found at these angles ( $2\theta = 38.39^\circ, 44.75^\circ, 65.96^\circ, 77.84^\circ$ ) at the Crystal Planes (111), (200), (220), and (311), respectively, with a space group Fm-3m no.225. The dimensions were  $a=b=c=4.0699 \text{ \AA}$ , and the crystal angles were  $\alpha=\beta=\gamma =$

$90^\circ$ . The energy was 700 mJ, which corresponds to the standard card (JCPDS 01-1172). This is due to the fact that at high energies, 700mJ the laser generates heat that is sufficient to form the cubic phase of Au NPs [19].

High energies are used to ablate the material in order to adjust the size of the crystals and particles and to examine the various crystallinities of the nanoparticles. The absence of any additional peaks suggests that the Au-NPs that were obtained are pure. According to the findings, Au-NPs maintain the same cubic phase during their crystalline development., as shown in Fig. 1.

#### X- Ray Diffraction for Copper

By analyzing the X-ray diffraction spectrum, one may comprehend the crystalline growth nature of thin films formed by the solid phase on a glass substrate at an annealing temperature of  $300^\circ\text{C}$ . In Fig 2, Cu nanoparticles are shown. In a single phase, it produces a monoclinic structure. The lattice's parameters are  $a = 4.84 \text{ \AA}$ ,  $b = 3.47 \text{ \AA}$ , and  $c = 5.33 \text{ \AA}$ . Peak locations and intensities are fairly consistent with the data (JCPDS file No. 05-

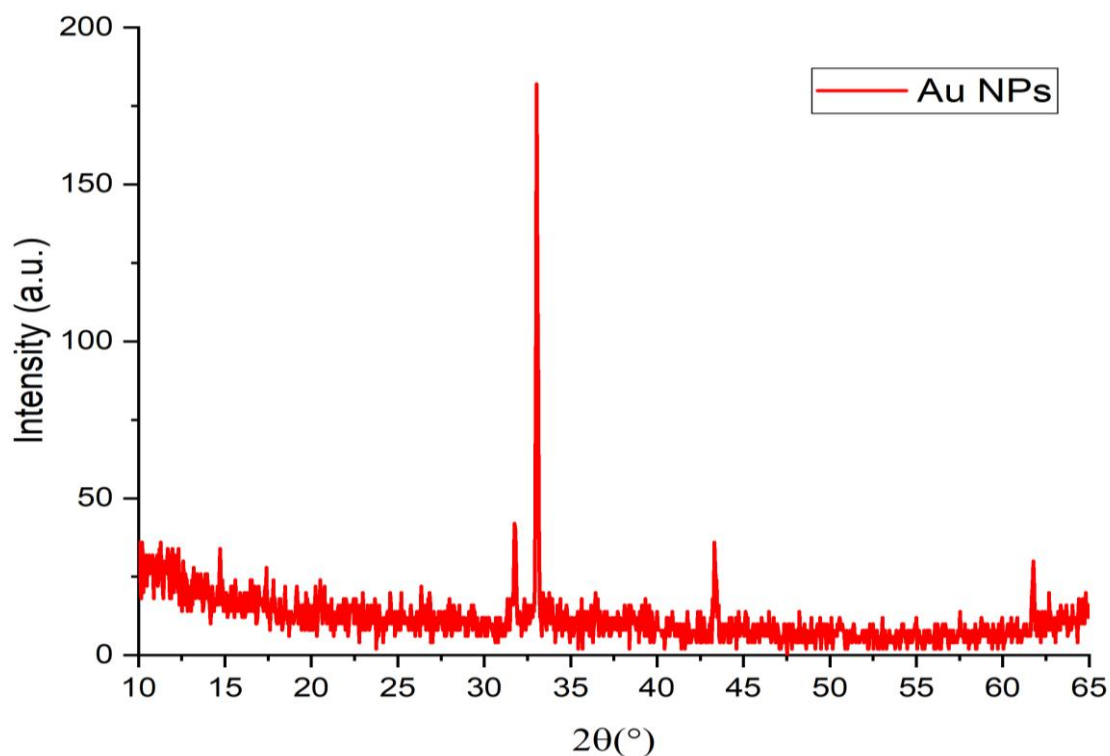


Fig. 1. X-ray diffraction patterns (XRD) for Au NPs.

661). According to planes (002) and (111), (222), and (113), in that order Using the Debye–Scherrer formula [20].

It was found that the average crystal size was 45 nm. Furthermore, the strongest peak was

discovered at  $2\theta = 35.45^\circ$ , which is in line with the diffractions of spherical nanoparticles formed in the structure with the [002] lattice plane.

Xrd for Cu/Au core/shell all reflections are similar to monometallic Cu and Au nanoparticles.

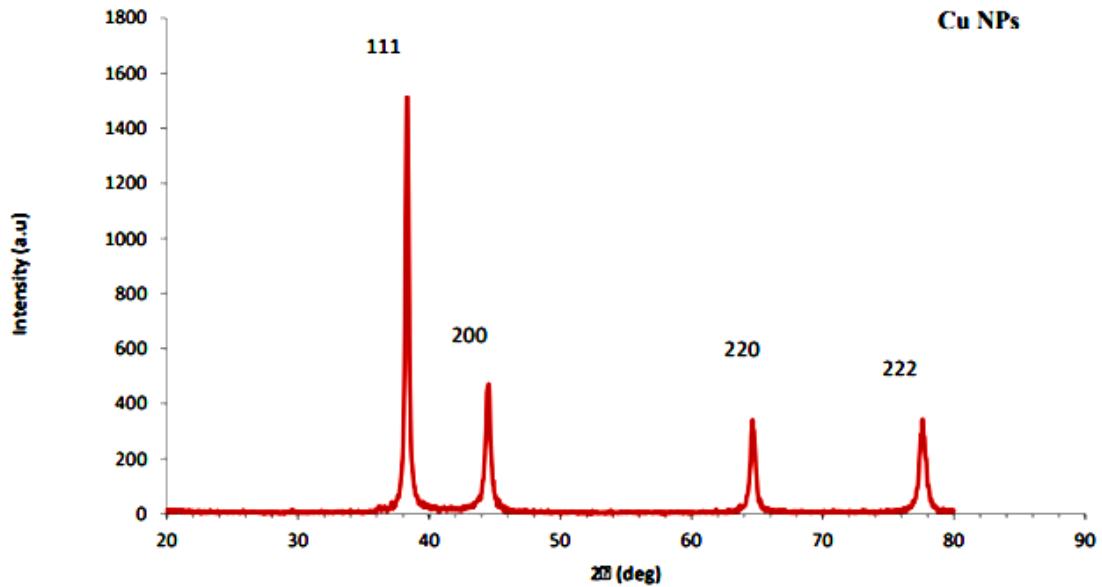


Fig. 2. X-ray diffraction patterns (XRD) for Cu NPs.

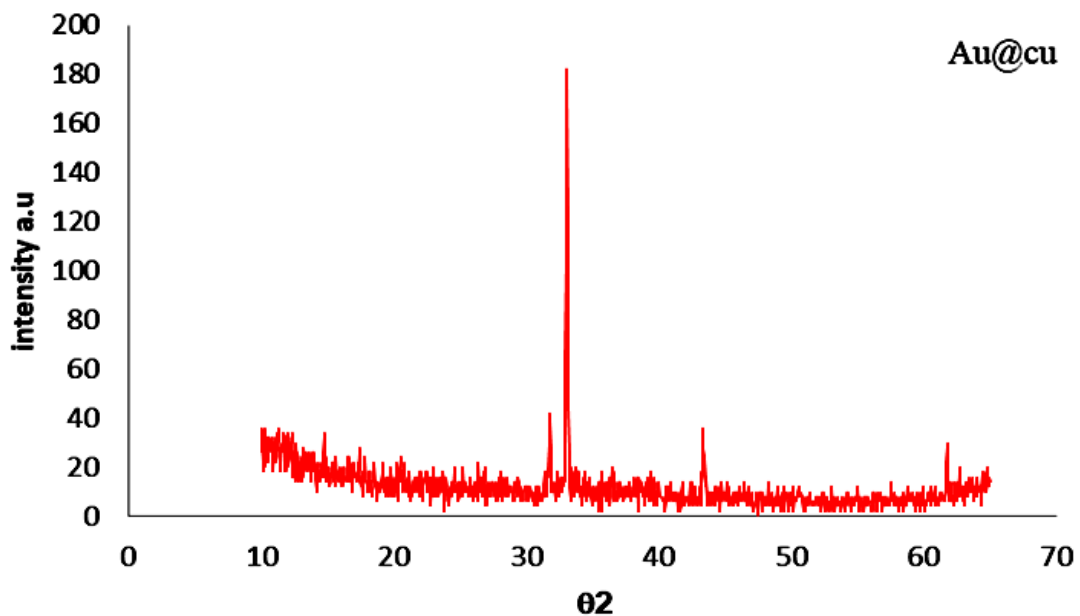


Fig. 3. X-ray diffraction patterns (XRD) for Au@Cu NPs.

Fig. 3 shows two abroad band at 42.47oand 49.41 (2θ) that can be attributed to the (111) and (200) crystallographic planes of Cu nanoparticles, the Cu NPs agreement with the JCPDS standard card No. (#96-901-3024). The peaks (111),(200),(220) and (311) planes that peaks at (2θ=38.20°,44.20°,63.98°and 78.02°) for Au NPs which agreement with the JCPDS standard card

No. 96-901-2431

*UV-Visible spectroscopy*

One technique for figuring out how much light is absorbed and scattered by a sample is UV-visible spectroscopy. The optical characteristics of nanoparticles are crucial for determining precise details on their size, shape, concentration, and

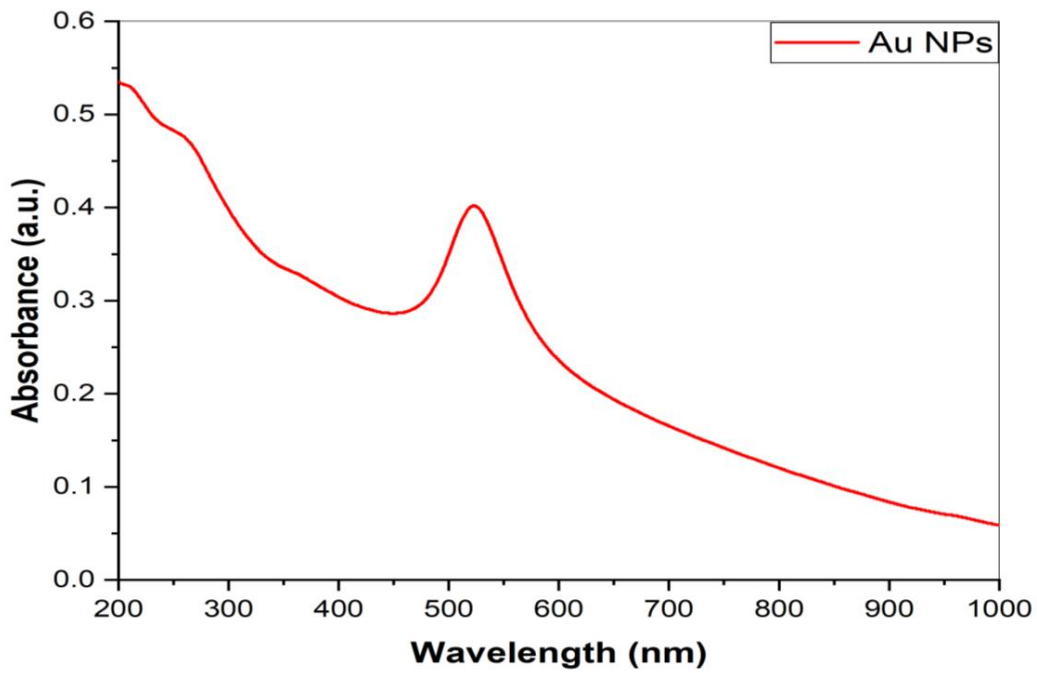


Fig. 4. UV for Au NPs.

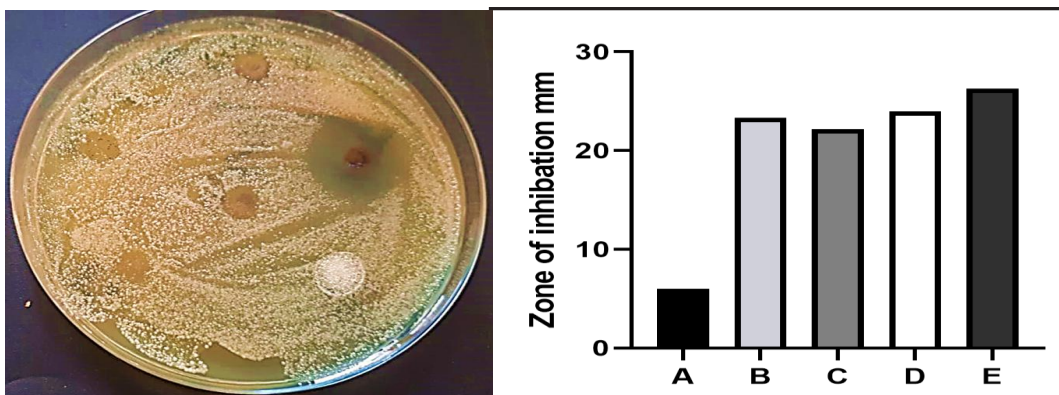


Fig. 5. UV for Au@Cu NPs.

agglomeration state. The UV-visible spectra of Au-NPs synthesized at 700 mJ with a continuous pulse of 1000 pulses are displayed in Fig. 4. For Au-NPs, the spectra show an absorption band characteristic with a peak at about 521–523 nm. This corresponds to gold's SPR. [21].

Because the NPs in solution are primarily spherical in shape and do not aggregate, there is just one SPR peak. As laser energy increased, so did the Plasmon peak's value. The concentration of NPs in suspension determines the intensity of the SPR peak; hence, a larger concentration of NPs results in a higher absorbance value. [22].

The UV-Spectra recorded from the colloidal solution (strong red color of Au-NPs) This Fig. 5 shows a typical Plasmon band which appeared a single but strong absorption peak centered at about 524.5 nm.

#### Bacterial Samples Preparation

The bacterial strains used in this study were *Escherichia coli*, which is Gram-negative, and *Staphylococcus aureus*, which is Gram-positive. They were ordered from the Ministry of Science and Technology's contamination research center in Bagdad, Iraq. The cultures of these two bacteria were cultivated on a nutrient agar plate at 37°C. Using a sterile loop, one colony was removed from the plate and put in 10 milliliters of nutritional broth. It was then incubated for the entire night at 37°C. After that, samples with concentrations of *Staphylococcus aureus* and *Escherichia coli* in each medium ranging from 1 to 108 cfu/mL were centrifuged for five minutes at 6000 rpm. After discarding the supernatants, the cells were suspended in 500 µL of phosphate-buffered saline (PBS) and centrifuged three times to guarantee

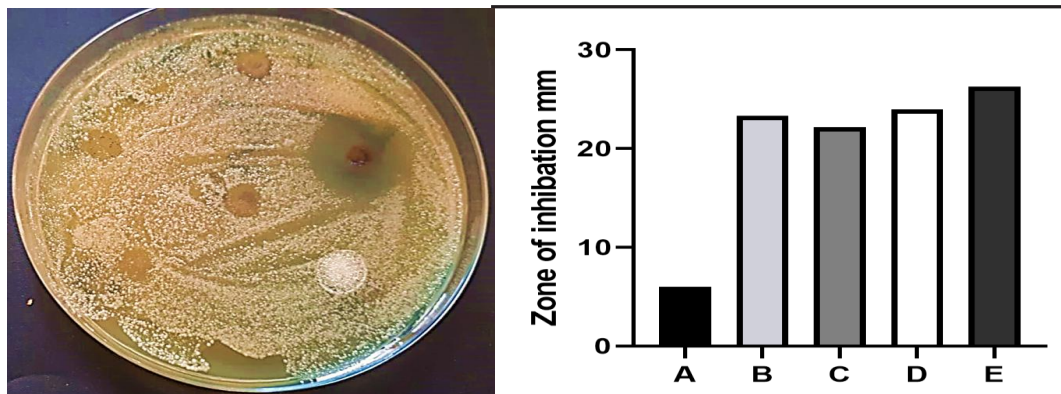


Fig. 6. Antibacterial activity of (N1) against *E. coli*. A, control. B, 25%. C, 50%. D, 75%. E, 100%.

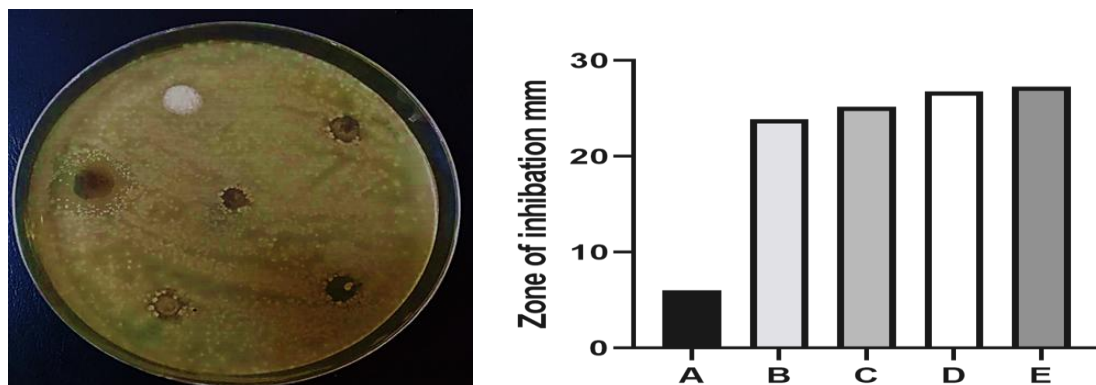


Fig. 7. Antibacterial activity of (N2) against *E. coli*. A, control. B, 25%. C, 50%. D, 75%. E, 100%.

that all media and debris were removed. Following the removal of the last wash's supernatant step, the cells were suspended in 50  $\mu$ L of PBS and mixed by pipetting to assure even cell distribution before delivery to the substrate.

**Antibacterial activity**

Using the agar well diffusion assay, the antibacterial activity of the synthesized X-SUBSTANCES was examined against strains of

Gram-positive (*S. aureus*) and Gram-negative (*E. Coli*) bacteria [23, 26]. Aseptically, 20 milliliters of Muller-Hinton (MH) agar were transferred into sterile Petri dishes. A sterile wire loop was used to extract the bacterial species from their stock cultures [27–28]. Following the organisms' culture, sterile tips were used to bore wells with a diameter of 6 mm into the agar plates. Various X-SUBSTANCES concentrations were used in the bored wells. Prior to measuring and documenting

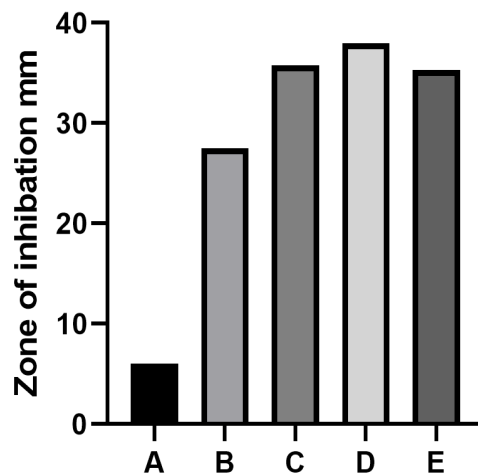
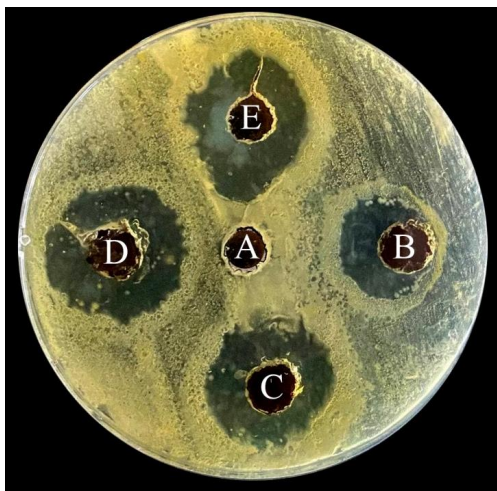


Fig. 8. Antibacterial activity of (N1) against *S.aureus*. A, control. B, 25%. C, 50%. D, 75%. E, 100%.

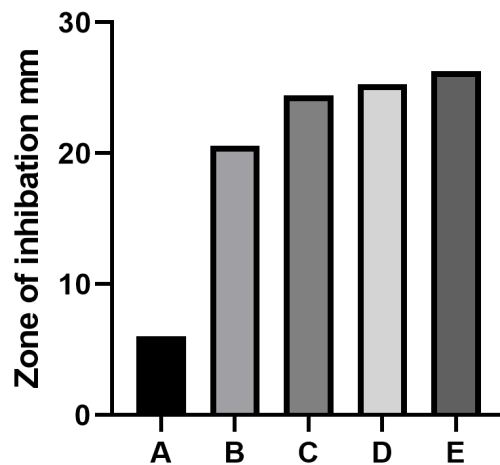
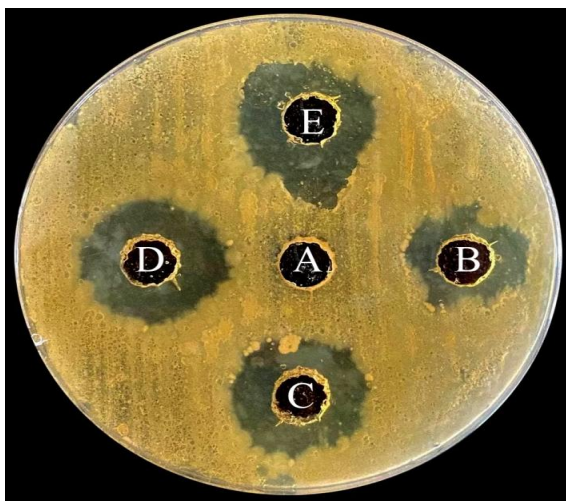


Fig. 9. Antibacterial activity of (N2) against *S.aureus*. A, control. B, 25%. C, 50%. D, 75%. E, 100%.

the average zones of inhibition diameter, the cultivated plates containing the test organisms and X-SUBSTANCES were incubated for an entire night at 37°C. [29].

#### Statistical analysis

Data were statically analysis using Graphpad prism program [30-31]. Data are represented as mean ± SD of three experiments. Indicate statistically significant difference at p<0.05 as shown in Figs. 6-9.

#### CONCLUSION

Numerous investigations have demonstrated that there are chemical, physical, and biological methods for creating copper and gold nanoparticles. The chemical and physical approaches are laborious and time-consuming. Moreover, certain chemical procedures include usage of dangerous compounds, which may inflict unwanted effects to the user. Therefore, quick, simple, and environmentally friendly procedures are required. An attempt to do so is biological synthesis. Research on the bioactivities of copper nanoparticles shown how well they worked against a variety of harmful bacteria, fungus, and algae.

#### CONFLICT OF INTEREST

The authors declare that there is no conflict of interests regarding the publication of this manuscript.

#### REFERENCES

1. Sengani M, Grumezescu AM, Rajeswari VD. Recent trends and methodologies in gold nanoparticle synthesis – A prospective review on drug delivery aspect. *OpenNano*. 2017;2:37-46.
2. Herizchi R, Abbasi E, Milani M, Akbarzadeh A. Current methods for synthesis of gold nanoparticles. *Artificial Cells, Nanomedicine, and Biotechnology*. 2014;44(2):596-602.
3. Mohazzab BF, Jaleh B, Nasrollahzadeh M, Issaabadi Z, Varma RS. Laser ablation-assisted synthesis of GO/TiO<sub>2</sub>/Au nanocomposite: Applications in K<sub>3</sub>[Fe(CN)<sub>6</sub>] and Nigrosin reduction. *Molecular Catalysis*. 2019;473:110401.
4. Nancy P, Nair AK, Antoine R, Thomas S, Kalarikkal N. In Situ Decoration of Gold Nanoparticles on Graphene Oxide via Nanosecond Laser Ablation for Remarkable Chemical Sensing and Catalysis. *Nanomaterials (Basel, Switzerland)*. 2019;9(9):1201.
5. Hernández-Maya M, Rivera-Quintero P, Ospina R, Quintero-Orozco JH, García-Castro AC. Ablation energy, water volume and ablation time: Gold nanoparticles obtained through by pulsed laser ablation in liquid. *Journal of Physics: Conference Series*. 2019;1386(1):012062.
6. Alluhaybi HA, Ghoshal SK, Shamsuri WNW, Alsobhi BO, Salim AA, Krishnan G. Pulsed laser ablation in liquid assisted growth of gold nanoparticles: Evaluation of structural and optical features. *Nano-Structures & Nano-Objects*. 2019;19:100355.
7. Kuriakose AC, Nampoori VPN, Thomas S. Facile synthesis of Au/CdS core-shell nanocomposites using laser ablation technique. *Mater Sci Semicond Process*. 2019;101:124-130.
8. Letzel A, Gökce B, Menzel A, Plech A, Barcikowski S. Primary particle diameter differentiation and bimodality identification by five analytical methods using gold nanoparticle size distributions synthesized by pulsed laser ablation in liquids. *Appl Surf Sci*. 2018;435:743-751.
9. Naharuddin NZA, Sadrolhosseini AR, Abu Bakar MH, Tamchek N, Mahdi MA. Laser ablation synthesis of gold nanoparticles in tetrahydrofuran. *Optical Materials Express*. 2020;10(2):323.
10. Bailly A-L, Correard F, Popov A, Tselikov G, Chaspoul F, Appay R, et al. In vivo evaluation of safety, biodistribution and pharmacokinetics of laser-synthesized gold nanoparticles. *Scientific reports*. 2019;9(1):12890-12890.
11. Daruich De Souza C, Ribeiro Nogueira B, Rostelato MECM. Review of the methodologies used in the synthesis gold nanoparticles by chemical reduction. *J Alloys Compd*. 2019;798:714-740.
12. Riedel R, Mahr N, Yao C, Wu A, Yang F, Hampp N. Synthesis of gold–silica core–shell nanoparticles by pulsed laser ablation in liquid and their physico-chemical properties towards photothermal cancer therapy. *Nanoscale*. 2020;12(5):3007-3018.
13. Kong F-Y, Zhang J-W, Li R-F, Wang Z-X, Wang W-J, Wang W. Unique Roles of Gold Nanoparticles in Drug Delivery, Targeting and Imaging Applications. *Molecules (Basel, Switzerland)*. 2017;22(9):1445.
14. Simon J, Nampoori VPN, Kailasnath M. Facile synthesis of Au-Ag core shell and nanoalloy using femtosecond laser ablation and their optical characterization. *Optik*. 2019;195:163168.
15. Arvinte A, Crudu I-A, Doroftei F, Timpu D, Pinteala M. Electrochemical codeposition of silver-gold nanoparticles on CNT-based electrode and their performance in electrocatalysis of dopamine. *J Electroanal Chem*. 2018;829:184-193.
16. Khalil I, Julkapli NM, Yehye WA, Basirun WJ, Bhargava SK. Graphene-Gold Nanoparticles Hybrid-Synthesis, Functionalization, and Application in a Electrochemical and Surface-Enhanced Raman Scattering Biosensor. *Materials (Basel, Switzerland)*. 2016;9(6):406.
17. Patil MP, Kim G-D. Eco-friendly approach for nanoparticles synthesis and mechanism behind antibacterial activity of silver and anticancer activity of gold nanoparticles. *Appl Microbiol Biotechnol*. 2016;101(1):79-92.
18. Chen Q, Ye Y, Liu J, Wu S, Li P, Liang C. Stability evolution of ultrafine Ag nanoparticles prepared by laser ablation in liquids. *J Colloid Interface Sci*. 2021;585:444-451.
19. Menazea AA, Abdelghany AM. Precipitation of silver nanoparticle within silicate glassy matrix via Nd:YAG laser for biomedical applications. *Radiat Phys Chem*. 2020;174:108958.
20. Torrisi A, Cutroneo M, Torrisi L, Vacík J. Biocompatible nanoparticles production by pulsed laser ablation in liquids. *Journal of Instrumentation*. 2020;15(03):C03053-C03053.
21. Torrisi L. Physical aspects of gold nanoparticles as cancer killer therapy. *Indian Journal of Physics*. 2020;95(2):225-234.

22. Jamaludin N, Chaudhary KT, Haider Z, Duralim M, Ismail FD, Roslan MS, et al. Effect of laser energy and wavelength on average size of gold nanoparticles synthesized by pulsed laser ablation in deionized water. *Journal of Physics: Conference Series*. 2020;1484(1):012029.
23. Tan MISMH, Omar AF, Rashid M, Hashim U. VIS-NIR spectral and particles distribution of Au, Ag, Cu, Al and Ni nanoparticles synthesized in distilled water using laser ablation. *Results in Physics*. 2019;14:102497.
24. De Giacomo A, Gaudiuso R, Koral C, Dell'Aglio M, De Pascale O. Nanoparticle-Enhanced Laser-Induced Breakdown Spectroscopy of Metallic Samples. *Anal Chem*. 2013;85(21):10180-10187.
25. Ulwali RA, Abbas HK, Karam AJ, Al-Zuky AA, Al-Kadhemy MFH, Al-Saleh AH. Surface Plasmon Resonance (SPR) Simulation of a Gold-Bismuth Bi-layer Gas Sensor. *Iraqi Journal of Science*. 2022;3402-3411.
26. Mohammed MKA, Mohammad MR, Jabir MS, Ahmed DS. Functionalization, characterization, and antibacterial activity of single wall and multi wall carbon nanotubes. *IOP Conference Series: Materials Science and Engineering*. 2020;757(1):012028.
27. Ali IH, Jabir MS, Al-Shmgani HSA, Sulaiman GM, Sadoon AH. Pathological And Immunological Study On Infection With Escherichia Coli In ale BALB/c mice. *Journal of Physics: Conference Series*. 2018;1003:012009.
28. Luksic I. Global and Regional Estimates of The Incidence and Case-Fatality Rates of Childhood Bacterial Meningitis Caused By Streptococcus Pneumoniae. *Morressier*; 2016.
29. Kadhemi SJ. Preparation of Al<sub>2</sub>O<sub>3</sub> /PVA Nanocomposite Thin Films by a Plasma Jet Method. *Science and Technology Indonesia*. 2023;8(3):471-478.
30. Fadhil WA, Jabbar II, Ali EH, Sulaiman GM, Khan RA, Mohammed HA. Freshly Prepared Graphene Oxide Nanoparticles' Wound-Healing Potential and Antibacterial Activity Specifically Against Staphylococcus aureus: In Vivo Efficacy and Clinical Isolate Evaluation. *Plasmonics*. 2024;20(2):763-773.
31. Rahmah MI, Saadoon NM, Mohasen AJ, Kamel RI, Fayad TA, Ibrahim NM. Double hydrothermal synthesis of iron oxide/silver oxide nanocomposites with antibacterial activity. *Journal of the Mechanical Behavior of Materials*. 2021;30(1):207-212.